

# Revealing universal Majorana fractionalization using differential shot noise and conductance in nonequilibrium states controlled by tunneling phases

Sergey Smirnov

*P. N. Lebedev Physical Institute of the Russian Academy of Sciences, 119991 Moscow, Russia\**

(Dated: May 27, 2022)

Universal fractionalization of quantum transport characteristics in Majorana quantum dot devices is expected to emerge for well separated Majorana bound states. We show that the Majorana universality of the differential shot noise  $\partial S^>/\partial V$  and conductance  $\partial I/\partial V$  at low bias voltages  $V$  arises only in ideal setups with only one Majorana mode entangled with the quantum dot. In realistic devices, where both Majorana modes are entangled with the quantum dot,  $\partial S^>/\partial V$  and  $\partial I/\partial V$  become very sensitive to tunneling phases and their universal fractional values are hard to observe even for well separated Majorana bound states. In contrast, as revealed here, the ratio  $(\partial S^>/\partial V)/(\partial I/\partial V)$  weakly depends on the tunneling phases and is fractional when the Majorana bound states are well separated or integer when they significantly overlap. Importantly, for very large  $V$  we demonstrate that this ratio becomes fully independent of the tunneling phases and its universal fractional Majorana value may be observed in state-of-the-art experiments.

## I. INTRODUCTION

Reliable access to electronic degrees of freedom fractionalized by formation of essentially nonlocal non-Abelian Majorana bound states (MBSs) [1] in a topological superconductor (TS) is an appealing goal which to some extent dates back to searching particles being their own antiparticles [2]. At present Majorana fractionalization is of fundamental importance for exploring universal properties of condensed matter systems [3–6], where MBSs appear in topologically nontrivial phases, and for practical implementation of topologically protected qubits involved in anyonic quantum computing [7].

One way to access MBSs is via quantum transport characteristics sensitive to fractionalizations of electronic degrees of freedom. Here average electric, thermoelectric and heat currents [8–22] provide valuable characteristics of MBSs. Also dynamics of average magnetizations [23] provides an alternative approach to study MBSs within quantum transport experiments. Qualitatively distinct and much more detailed quantum transport information about MBSs is encoded in shot and quantum noise which directly scans universal fractional character of excitations in nonequilibrium states [24–32]. In particular, Majorana shot noise taking into account continuum quasiparticles in tunnel junctions [33], giant Majorana shot noise in topological trijunctions [34] and full braiding Majorana protocols obtained from weak measurements based on shot noise statistics [35] demonstrate impressively diverse aspects of Majorana physics beyond mean electric currents. Another opportunity which is fundamentally different from quantum transport is to uniquely probe fractionalization via quantum thermodynamic characteristics such as the entropy. Indeed, well separated MBSs

in nanoscopic setups result in fractional plateaus [36–40] of the entropy. Ongoing elaboration of experimental techniques and successful measurements of the entropy [41–46] have established a convincing basis for a future thermodynamic access to MBSs.

Due to well established technology to measure, *e.g.* electric currents, quantum transport in nanoscopic setups is relatively simpler to perform than quantum thermodynamics. In particular, measurements of mean electric currents in setups presumably involving MBSs provide corresponding electric conductances [47]. Unfortunately, this most straightforward way to probe MBSs is unreliable [48–50]. Thus other approaches, based preferably on directly and simply measurable quantities, are required to access MBSs beyond mean electric currents.

Here we demonstrate how one can access MBSs via directly measurable observables such as differential shot noise and conductance in realistic Majorana quantum dot (QD) devices. To avoid unreliable measurements [48] in ideal setups, involving only one end of a TS, it is necessary to probe MBSs simultaneously at both ends. Fractionalization in such devices is driven by processes entangling a QD with both Majorana modes. Such an entanglement may also be engineered for implementing Majorana qubits [51, 52] or even accidentally induced during a technological process used to prepare a setup. We show that under such circumstances the expected universal Majorana properties of the differential shot noise and conductance are washed out by the Majorana tunneling phases even for well separated MBSs. Thus each of these observables alone does not straightforwardly indicate that in fact one deals with MBSs. This creates a general problem because in majority of experimental setups precise values of the tunneling phases are hard to extract. Remarkably, as we demonstrate, in contrast to the differential shot noise and conductance, the ratio of these two observables weakly depends on the tunneling phases. More importantly, we find that it takes fractional values for well separated MBSs and becomes integer when the MBSs merge into a single Dirac fermion. Thus this ratio

\* 1) sergej.physik@gmail.com

2) sergey.smirnov@physik.uni-regensburg.de

3) ssmirnov@sci.lebedev.ru

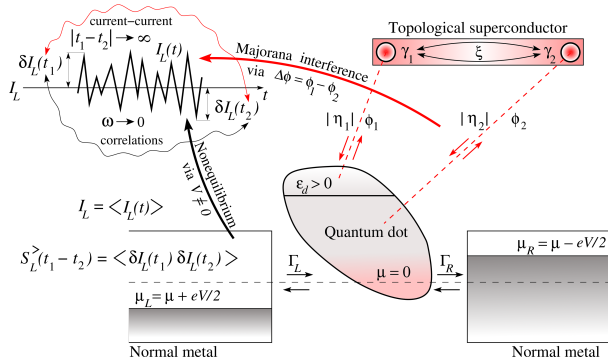


FIG. 1. A quantum device entangling both MBSs with external degrees of freedom. Due to this entanglement physical properties of the device, in particular quantum transport characteristics, such as its shot noise and conductance, strongly depend on the Majorana tunneling phases.

provides a straightforward access to fractionalization in Majorana QD devices.

Furthermore, a detailed numerical analysis of the dependences of the differential shot noise and conductance on the tunneling phases and bias voltage reveals a fine structure of their resonances. Using these resonances one can extract all the Majorana tunneling parameters including the tunneling phases. The dependence on these parameters also suggests a way to shift the Majorana resonances to higher bias voltages where it will be simpler to detect them in experiments.

The paper is organized as follows. In Section II we present the physical model of a feasible experimental setup which admits measurements of quantum transport observables such as its differential shot noise and conductance. Numerical results obtained for these observables are explored in Section III. We conclude the paper with Section IV where it is shown that the Majorana universal fractionalization at high bias voltages may be accessed in experiments performed at high temperatures achievable in modern labs.

## II. MAJORANA QUANTUM DOT SETUP, ITS DIFFERENTIAL SHOT NOISE AND CONDUCTANCE

To quantitatively analyze how an entanglement of a QD with both Majorana modes is revealed in fluctuations and the mean value of the electric current, flowing through the QD, we consider the setup in Fig. 1. The schematic setup in Fig. 1 is fully sufficient for our main goal, that is for the theoretical analysis presented below. However, it is important to note that an experimental realization of this theoretical model is feasible. For example, it can be implemented using an InAs nanowire with an epitaxial Al layer grown on a part of the nanowire's surface [53, 54]. Here, the Al shell is etched on one end of the nanowire to prepare a bare InAs segment where

afterwards a QD is formed. Thus in this technological process the TS is located with respect to the QD in an essentially asymmetric way: one end of the TS is much closer to the QD than the other one. As a result, the first Majorana mode  $\gamma_1$  is coupled to the QD stronger than the second Majorana mode  $\gamma_2$ , that is  $|\eta_1| > |\eta_2|$  (see below for more details). The setup in Ref. [54] may be adapted to our theoretical model by forming near the QD two normal metallic contacts whose coupling strength  $\Gamma$  (see below for more details) may be varied by the voltage on gates located between the contacts and QD. An alternative location of the TS with respect to the QD is used in Ref. [8] and assumes a curved shape of the TS. In such a curved setup both  $|\eta_1|$  and  $|\eta_2|$  are assumed to be controllable and thus one can have both situations  $|\eta_1| > |\eta_2|$  and  $|\eta_1| \approx |\eta_2|$ . In particular, the regime  $|\eta_1| > |\eta_2|$  is used to implement driven dissipative Majorana qubits [51]. Below we will assume  $|\eta_1| > |\eta_2|$  since this situation is more relevant technologically as well as for practical purposes. We also note that while in the setup of Ref. [54] the phases  $\phi_{1,2}$  may have arbitrary fixed values induced during the technological process, in Ref. [8] the phases  $\phi_{1,2}$  are assumed to be externally controlled by a magnetic flux. Such an external control of  $\phi_{1,2}$  is also assumed for practical implementations of Majorana qubits [51]. Our theoretical analysis below is applicable to both of these situations and may be used to interpret experiments where the phases  $\phi_{1,2}$  are fixed or externally controlled.

To perform a theoretical analysis, we assume that the physical system includes a QD,

$$\hat{H}_d = \epsilon_d d^\dagger d, \quad (1)$$

with one nondegenerate energy level  $\epsilon_d$ , whose location may be tuned by a gate voltage. Although here the QD is spinless and thus Kondo correlations are absent, in the following we assume  $\epsilon_d \geq 0$  (for example, empty dot, see also Ref. [9]) in order to describe a universal regime induced solely by MBSs, that is excluding even for spin-degenerate QDs a possible interplay between universal Majorana fractionalizations and the universality induced by Kondo correlations [55–61] which would have emerged in the spin-degenerate case for  $\epsilon_d < 0$ . In practice the spinless model in Eq. (1) is realized, for example, in strong magnetic fields used to bring the TS into its topological phase. Under such circumstances interactions in the QD do not play a role and the non-interacting spinless model in Eq. (1) is an adequate tool to analyze Majorana signatures [62]. This has also been confirmed, for example in Ref. [63], using numerical renormalization group calculations showing a transition of the linear conductance from the low magnetic field plateau  $3e^2/2h$  to the high magnetic field plateau  $e^2/2h$  induced solely by the MBSs after the magnetic field has switched the QD into the spinless regime and thus made it non-interacting via eliminating the Kondo correlations. In spin-degenerate QDs interactions play an important role [64–68]. However, numerical renormalization group calculations indi-

cate (see, for example, Ref. [69]) that even in interacting spin-degenerate QDs Majorana induced fractionalizations may decouple from Kondo correlations. Thus interacting spin-degenerate QDs coupled to MBSs may behave as their non-interacting counterparts. In particular, the low-temperature entropies in interacting and non-interacting spin-degenerate QDs coupled to MBSs are identical and may be obtained using non-interacting spin-degenerate QDs coupled to MBSs [69]. Thus even for spin-degenerate cases one may consider non-interacting QDs coupled to MBSs to explore Majorana induced properties at low temperatures, for example, Majorana shot noise as has been done in Ref. [32].

The setup also involves left ( $L$ ) and right ( $R$ ) contacts, which are normal metals,

$$\hat{H}_c = \sum_{l=L,R} \sum_k \epsilon_k c_{lk}^\dagger c_{lk}, \quad (2)$$

with continuum spectra approximated by a constant density of states,  $\nu(\epsilon) \approx \nu_c/2$ , in the range of energies relevant for quantum transport, and a grounded one-dimensional TS,

$$\hat{H}_{ts} = i\xi\gamma_2\gamma_1/2, \quad (3)$$

whose low-energy properties are governed by MBSs,  $\gamma_{1,2}^\dagger = \gamma_{1,2}$ ,  $\{\gamma_i, \gamma_j\} = 2\delta_{ij}$ , localized at its ends and having a finite overlap,  $\xi \neq 0$ . The contacts' Fermi-Dirac distributions,

$$n_{L,R}(\epsilon) = \frac{1}{\exp\left[\frac{\epsilon - \mu_{L,R}}{k_B T}\right] + 1}, \quad (4)$$

are specified by the contacts' temperature  $T$  and chemical potentials  $\mu_{L,R} = \mu \pm eV/2$ , where  $V$  is the bias voltage. The QD is coupled to the contacts and TS via tunneling processes,

$$\begin{aligned} \hat{H}_{d\leftrightarrow c} &= \sum_{l=L,R} \mathcal{T}_l \sum_k c_{lk}^\dagger d + \text{H.c.}, \\ \hat{H}_{d\leftrightarrow ts} &= \eta_1^* d^\dagger \gamma_1 + \eta_2^* d^\dagger \gamma_2 + \text{H.c.}, \end{aligned} \quad (5)$$

where  $\eta_{1,2} = |\eta_{1,2}| \exp(i\phi_{1,2})$  and we assume  $|\eta_1| > |\eta_2|$ . The interaction between the QD and contacts is characterized by the tunneling energy  $\Gamma \equiv \Gamma_L + \Gamma_R$ ,  $\Gamma_{L,R} \equiv \pi\nu_c |\mathcal{T}_{L,R}|^2$ , and for simplicity we assume  $\Gamma_L = \Gamma_R$ . When  $V \neq 0$ , different chemical potentials,  $\mu_L \neq \mu_R$ , induce nonequilibrium which essentially determines the electric current, in particular, its mean value and random deviations from it. The MBSs  $\gamma_1$  and  $\gamma_2$  tunnel to the QD with different phases,  $\phi_1 \neq \phi_2$ , inducing on the QD an interference controlled by the phase difference  $\Delta\phi = \phi_1 - \phi_2$  which also essentially determines the mean value and fluctuations of the electric current.

Having the full Hamiltonian,  $\hat{H} = \hat{H}_d + \hat{H}_c + \hat{H}_{ts} + \hat{H}_{d\leftrightarrow c} + \hat{H}_{d\leftrightarrow ts}$ , one may consider various observables using, *e.g.*, the Keldysh field integral formalism [70] particularly convenient to treat stationary nonequilibrium.

Within this formalism the second quantized fermionic operators are replaced by the Grassmann fields,  $\psi(t)$ ,  $\phi_{lk}(t)$ ,  $\zeta(t)$ , corresponding to the QD, contacts and TS, respectively. The electric current operator in the  $l$ -th contact is expressed through the Grassmann fields on the forward ( $q = +$ ) or backward ( $q = -$ ) branch of the Keldysh contour,

$$I_{lq}(t) = (ie/\hbar) \sum_k [\mathcal{T}_l \bar{\phi}_{lkq}(t) \psi_q(t) - \text{G.c.}], \quad (6)$$

where G.c. denotes the Grassmann conjugation. The Hamiltonians in Eqs. (1)-(3) are replaced by the corresponding Keldysh actions of the isolated QD, contacts and TS,  $S_d$ ,  $S_c$  and  $S_{ts}$ , which are of conventional  $2 \times 2$  matrix form in the retarded-advanced space. The Hamiltonians in Eq. (5) are replaced by the following actions:

$$\begin{aligned} S_{d\leftrightarrow c} &= - \int_{-\infty}^{\infty} dt \sum_{l=L,R} \sum_k \{ \mathcal{T}_l [\bar{\phi}_{lk+}(t) \psi_+(t) \\ &\quad - \bar{\phi}_{lk-}(t) \psi_-(t)] + \text{G.c.} \}, \\ S_{d\leftrightarrow ts} &= - \int_{-\infty}^{\infty} dt \{ \eta_1^* [\bar{\psi}_+(t) \zeta_+(t) + \bar{\psi}_+(t) \bar{\zeta}_+(t) \\ &\quad - \bar{\psi}_-(t) \zeta_-(t) - \bar{\psi}_-(t) \bar{\zeta}_-(t)] + i\eta_2^* [\bar{\psi}_+(t) \zeta_+(t) \\ &\quad + \bar{\psi}_-(t) \bar{\zeta}_-(t) - \bar{\psi}_-(t) \zeta_-(t) - \bar{\psi}_+(t) \bar{\zeta}_+(t)] + \text{G.c.} \}. \end{aligned} \quad (7)$$

To generate the mean electric current and various current-current correlators one also adds the current action,

$$S_I[J_{lq}(t)] = - \int_{-\infty}^{\infty} dt \sum_{l=L,R} \sum_{q=+,-} J_{lq}(t) I_{lq}(t), \quad (8)$$

with the source fields  $J_{lq}(t)$ . The full Keldysh action,  $S_K[J_{lq}(t)] = S_d + S_c + S_{ts} + S_{d\leftrightarrow c} + S_{d\leftrightarrow ts} + S_I[J_{lq}(t)]$ , determines the Keldysh generating functional,

$$Z[J_{lq}(t)] = \int \mathcal{D}[\bar{\psi}_q, \psi_q; \bar{\phi}_{lkq}, \phi_{lkq}; \bar{\zeta}_q, \zeta_q] e^{\frac{i}{\hbar} S_K[J_{lq}(t)]}, \quad (9)$$

from which one, *e.g.*, generates

$$\begin{aligned} \langle I_{lq}(t) \rangle_{S_K} &= i\hbar \frac{\delta Z[J_{lq}(t)]}{\delta J_{lq}(t)} \Big|_{J_{lq}(t)=0}, \\ \langle I_{lq}(t) I_{l'q'}(t') \rangle_{S_K} &= (i\hbar)^2 \frac{\delta^2 Z[J_{lq}(t)]}{\delta J_{lq}(t) \delta J_{l'q'}(t')} \Big|_{J_{lq}(t)=0}, \end{aligned} \quad (10)$$

where  $\langle \dots \rangle_{S_K}$  means averaging at  $J_{lq}(t) = 0$  that is with respect to the action  $S_K = S_K[J_{lq}(t) = 0]$ ,

$$\langle \dots \rangle_{S_K} = \int \mathcal{D}[\bar{\psi}_q, \psi_q; \bar{\phi}_{lkq}, \phi_{lkq}; \bar{\zeta}_q, \zeta_q] e^{\frac{i}{\hbar} S_K[\dots]}. \quad (11)$$

In the following we will focus on the left contact,  $l = L$ , and explore the mean electric current  $I(V, \Delta\phi) = \langle I_{Lq}(t) \rangle_{S_K}$  and the greater current-current correlator  $S^>(t, t'; V, \Delta\phi) = \langle \delta I_{L-}(t) \delta I_{L+}(t') \rangle_{S_K}$ ,  $\delta I_{Lq}(t) =$

$I_{LQ}(t) - I(V, \Delta\phi)$ . The Fourier transform of the correlator  $S^>(t, t'; V, \Delta\phi) = S^>(t - t'; V, \Delta\phi)$ ,

$$S^>(\omega; V, \Delta\phi) = \int_{-\infty}^{\infty} dt e^{i\omega t} S^>(t; V, \Delta\phi), \quad (12)$$

is an important quantity because at  $\omega = 0$  it specifies the shot noise  $S^>(V, \Delta\phi) \equiv S^>(\omega = 0; V, \Delta\phi)$ .

In experiments one directly measures the differential shot noise and conductance,  $\partial S^>(V, \Delta\phi)/\partial V$ ,  $\partial I(V, \Delta\phi)/\partial V$ , and below we focus on these partial derivatives. We obtain  $S^>(V, \Delta\phi)$  and  $I(V, \Delta\phi)$  via numerical integrations and then perform numerical differentiations. The regime where  $|\eta_1|$  prevails,  $|\eta_1| > \max\{|\epsilon_d|, |eV|, k_B T, \Gamma, |\eta_2|, \xi\}$ , is of particular interest for observing Majorana universality in experiments and below we explore it explicitly. As discussed above, the physical setup assumes that  $\Gamma$  may be enhanced or suppressed by the voltage on gates located between the QD and contacts. Our motivation for suppressing  $\Gamma$  below  $|\eta_1|$  is that for  $\Gamma < |\eta_1|$  the properties of the QD will be dominated by Majorana fractional character in a wide energy range. Physically this is expected because the tunneling of the MBSs into the QD is much stronger than the tunneling from the contacts whose non-fractional degrees of freedom could significantly wash out various Majorana fractionalizations in the opposite regime, that is for  $\Gamma > |\eta_1|$ . We also note that to get the numerical results presented below we specify all the energies in units of  $\Gamma$ . In particular, the bias voltage  $|eV|$  is varied in a wide range, from small to large values in units of  $\Gamma$ . However, since  $\Gamma$  is made very small using the gates mentioned above,  $|eV|$  will also be small even if it takes large values in units of  $\Gamma$ . This means that in our numerical results the bias voltage always remains small enough so that other levels of the QD are not relevant and our theoretical model provides a reasonable description of experiments.

### III. NUMERICAL RESULTS

In the upper panel of Fig. 2 we show  $\partial S^>/\partial V$  and  $\partial I/\partial V$  as functions of  $\Delta\phi$  for  $|eV|/\Gamma \ll 1$ . Both quantities exhibit resonances around  $\Delta\phi_{\text{res}} = 0, \pi, 2\pi$  where they reach their universal fractional values,  $\partial S^>/\partial V = e^3/4h$  and  $\partial I/\partial V = e^2/2h$ . However, due to strong dependences of  $\partial S^>/\partial V$  and  $\partial I/\partial V$  on  $\Delta\phi$  they quickly deviate from these fractional values which, thus, can be observed only in very narrow ranges of  $\Delta\phi$ . The left inset shows the fine structures of the resonances of  $\partial S^>/\partial V$  and  $\partial I/\partial V$  in the vicinity of  $\Delta\phi = \pi$ . As can be seen, these resonances are split into two peaks. We find numerically that the distances  $\Delta\phi_{I, \text{max}}$  and  $\Delta\phi_{S, \text{max}}$  between the peaks of  $\partial I/\partial V$  and  $\partial S^>/\partial V$ , respectively, depend on both  $|\eta_2|$  and  $|eV|$ ,

$$\Delta\phi_{I, \text{max}} = \frac{1}{2} \frac{|eV|}{|\eta_2|}, \quad \Delta\phi_{S, \text{max}} \sim \frac{\sqrt{\Gamma|eV|}}{|\eta_2|}. \quad (13)$$

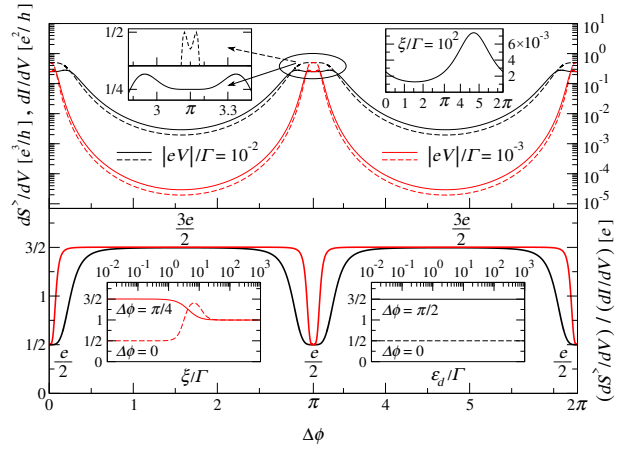


FIG. 2. Upper panel: Differential shot noise  $\partial S^>/\partial V$  (solid lines) and differential conductance  $\partial I/\partial V$  (dashed lines) as functions of the tunneling phase difference  $\Delta\phi$  for small bias voltages,  $|eV|/\Gamma \ll 1$ . The black curves correspond to the case  $|eV|/\Gamma = 10^{-2}$  while the red curves correspond to the case  $|eV|/\Gamma = 10^{-3}$ . The other parameters are the same for the two cases:  $\epsilon_d/\Gamma = 10$ ,  $k_B T/\Gamma = 10^{-6}$ ,  $|\eta_1|/\Gamma = 10^3$ ,  $|\eta_2|/\Gamma = 10^{-1}$ ,  $\xi/\Gamma = 10^{-4}$ . Lower panel: Black and red curves show the ratio  $(\partial S^>/\partial V)/(\partial I/\partial V)$  obtained from the corresponding curves in the upper panel.

These expressions are valid only when  $|eV| \gg k_B T$ . For  $|eV| \ll k_B T$  the resonance of the linear conductance also splits into two resonances with the distance between them depending on  $|\epsilon_d|$  as also confirmed by the entropy analysis [38]. In particular, for  $\epsilon_d = 0$  it is equal to  $\pi$  [8]. The right inset shows  $\partial S^>/\partial V$  and  $\partial I/\partial V$  for  $\xi/\Gamma \gg 1$  when the MBSs strongly overlap and form a single Dirac fermion. Specifically, in the inset  $\xi/\Gamma = 10^2$ . The two physical quantities,  $\partial S^>/\partial V$  and  $\partial I/\partial V$ , are strongly suppressed and coincide with each other leading to a single curve in the inset. Moreover, as the inset explicitly demonstrates, the strong overlap of the MBSs doubles the period of  $\partial S^>/\partial V$  and  $\partial I/\partial V$  from  $\pi$  to  $2\pi$ . The lower panel shows the ratio  $(\partial S^>/\partial V)/(\partial I/\partial V)$  corresponding to the black and red curves in the upper panel. In contrast to  $\partial S^>/\partial V$  and  $\partial I/\partial V$  their ratio is almost independent of  $\Delta\phi$ . Indeed, it has wide plateaus, on which it is equal to  $3e/2$ , and narrow antiresonances, corresponding to the resonances in the upper panel. The minimum of these antiresonances is also fractional, equal to  $e/2$ , while their width is determined by both the bias voltage  $|eV|$  and tunneling amplitude  $|\eta_2|$ . The left inset shows the ratio  $(\partial S^>/\partial V)/(\partial I/\partial V)$  as a function of  $\xi$  for the case  $|eV|/\Gamma = 10^{-3}$  and  $\Delta\phi = 0$  (dashed curve),  $\Delta\phi = \pi/4$  (solid curve). We see that both fractional values,  $3e/2$  and  $e/2$ , are observed for well separated MBSs, when  $\xi/\Gamma \ll 1$ . For strongly overlapping MBSs, when  $\xi/\Gamma \gg 1$ , the ratio takes the integer Dirac value,  $(\partial S^>/\partial V)/(\partial I/\partial V) = e$ , and becomes independent of  $\Delta\phi$ . The right inset shows for the case  $|eV|/\Gamma = 10^{-2}$  the universality of the two nontrivial Majorana fractional values,  $3e/2$  (solid curve,  $\Delta\phi = \pi/2$ ) and  $e/2$  (dashed

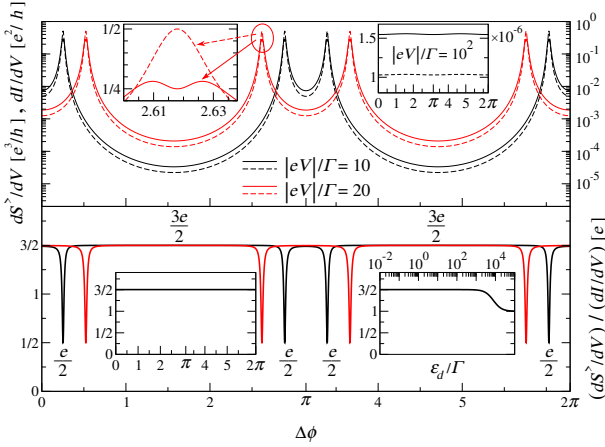


FIG. 3. Upper panel: Differential shot noise  $\partial S^>/\partial V$  (solid lines) and differential conductance  $\partial I/\partial V$  (dashed lines) as functions of the tunneling phase difference  $\Delta\phi$  for large bias voltages,  $|eV|/\Gamma \sim 10$ . The black curves correspond to the case  $|eV|/\Gamma = 10$  while the red curves correspond to the case  $|eV|/\Gamma = 20$ . The other parameters are the same for the two cases:  $\epsilon_d/\Gamma = 10$ ,  $k_B T/\Gamma = 10^{-6}$ ,  $|\eta_1|/\Gamma = 10^3$ ,  $|\eta_2|/\Gamma = 10$ ,  $\xi/\Gamma = 10^{-4}$ . Lower panel: Black and red curves show the ratio  $(\partial S^>/\partial V)/(\partial I/\partial V)$  obtained from the corresponding curves in the upper panel.

curve,  $\Delta\phi = 0$ ), that is their independence of the gate voltage controlling the value of  $\epsilon_d$ .

The differential shot noise and conductance for large bias voltages are shown as functions of  $\Delta\phi$  in the upper panel of Fig. 3. As in Fig. 2, the curves exhibit resonances with  $\partial S^>/\partial V = e^3/4h$  and  $\partial I/\partial V = e^2/2h$ . However, now  $\Delta\phi_{\text{res}} \neq 0, \pi, 2\pi$ . The new values of  $\Delta\phi_{\text{res}}$  are determined by both  $|eV|$  and  $|\eta_2|$ . Here, the value of  $|\eta_2|$  is increased in comparison with Fig. 2 in order to clearly show that the new locations of the resonances of both  $\partial S^>/\partial V$  and  $\partial I/\partial V$  are determined by  $\Delta\phi_{I,\text{max}}$  (and not by  $\Delta\phi_{S,\text{max}}$ ) in Eq. (13). The left inset shows that at large bias voltages there happens a qualitative change in the structure of the resonances in comparison with small bias voltages. Indeed, as can be seen in this inset, the resonance of  $\partial I/\partial V$  does not have any fine structure anymore and is characterized by a single peak. In contrast, the resonance of  $\partial S^>/\partial V$  has a fine structure: it is split into two peaks. From our numerical calculations we find that the distance between these two peaks depends on  $|\eta_2|$  and almost independent of  $|eV|$ ,

$$\Delta\phi_{S,\text{max}} \sim \frac{\Gamma}{|\eta_2|}. \quad (14)$$

The right inset shows  $\partial S^>/\partial V$  (solid curve) and  $\partial I/\partial V$  (dashed curve) as functions of  $\Delta\phi$  for very large bias voltage,  $|eV|/\Gamma = 10^2$ . As can be seen, at very large bias voltages both the differential shot noise and conductance are strongly suppressed,  $\partial S^>/\partial V \ll e^3/4h$ ,  $\partial I/\partial V \ll e^2/2h$ , and vary relatively weakly as functions of  $\Delta\phi$ . The curves in the lower panel demonstrate

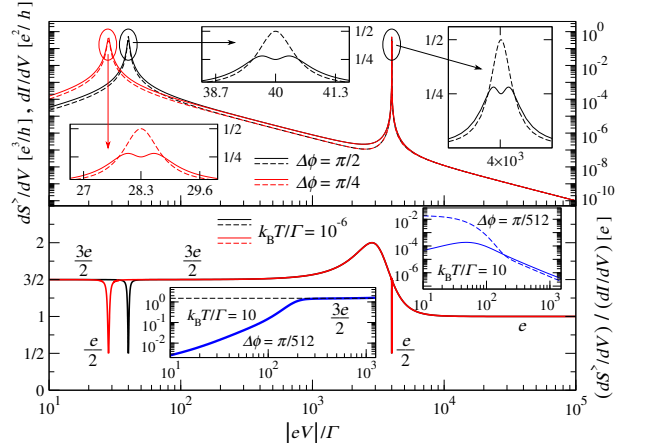


FIG. 4. Upper panel: Differential shot noise  $\partial S^>/\partial V$  (solid lines) and differential conductance  $\partial I/\partial V$  (dashed lines) as functions of the bias voltage  $|eV|$  for two values of the tunneling phase difference  $\Delta\phi$ . The black curves correspond to the case  $\Delta\phi = \pi/2$  while the red curves correspond to the case  $\Delta\phi = \pi/4$ . The other parameters are the same for the two cases:  $\epsilon_d/\Gamma = 10$ ,  $k_B T/\Gamma = 10^{-6}$ ,  $|\eta_1|/\Gamma = 10^3$ ,  $|\eta_2|/\Gamma = 10$ ,  $\xi/\Gamma = 10^{-4}$ . Lower panel: Black and red curves show the ratio  $(\partial S^>/\partial V)/(\partial I/\partial V)$  obtained from the corresponding curves in the upper panel.

the ratio  $(\partial S^>/\partial V)/(\partial I/\partial V)$  corresponding to the two bias voltages in the upper panel. As in Fig. 2, whereas  $\partial S^>/\partial V$  and  $\partial I/\partial V$  change relatively strongly (several orders of magnitude), their ratio exhibits weak dependence on  $\Delta\phi$  characterized by wide plateaus separated by narrow antiresonances. On the plateaus and at the minima of the antiresonances the ratio is fractional, equal to  $3e/2$  and  $e/2$ , respectively. The left inset shows the ratio  $(\partial S^>/\partial V)/(\partial I/\partial V)$  obtained from the curves in the right inset of the upper panel. We see that although at very large bias voltages ( $|eV|/\Gamma = 10^2$ ) both  $\partial S^>/\partial V$  and  $\partial I/\partial V$  are strongly suppressed, their ratio takes the Majorana fractional value  $3e/2$  in the whole range of  $\Delta\phi$ . The right inset demonstrates the universality (independence of  $\epsilon_d$ ) of the Majorana fractional value  $3e/2$  at very large bias voltages ( $|eV|/\Gamma = 10^2$ ). The curve in this inset is also independent of  $\Delta\phi$ . As expected, the Majorana universality takes place only at  $|\epsilon_d| \leq |\eta_1|$ .

The upper panel of Fig. 4 shows  $\partial S^>/\partial V$  and  $\partial I/\partial V$  as functions of  $V$  for two different values of  $\Delta\phi$ . Both  $\partial S^>/\partial V$  and  $\partial I/\partial V$  exhibit two resonances at  $|eV_{\text{res},1}|$  and  $|eV_{\text{res},2}|$  where they reach their universal fractional values,  $\partial S^>/\partial V = e^3/4h$  and  $\partial I/\partial V = e^2/2h$ . We find numerically that  $|eV_{\text{res},1}|$  depends only on  $|\eta_1|$  whereas  $|eV_{\text{res},2}|$  depends on both  $|\eta_2|$  and  $\Delta\phi$ ,

$$|eV_{\text{res},1}| = 4|\eta_1|, \quad |eV_{\text{res},2}| = 4|\eta_2|\sin(\Delta\phi). \quad (15)$$

Away from these resonances both  $\partial S^>/\partial V$  and  $\partial I/\partial V$  quickly deviate from their universal fractional values. The left and middle insets show the detailed profiles of the resonances at  $|eV_{\text{res},2}|$  for  $\Delta\phi = \pi/4$  and  $\Delta\phi = \pi/2$ ,

respectively, while the right inset shows the detailed profile of the resonances at  $|eV_{\text{res},1}|$ . These three insets all demonstrate that the resonances of  $\partial I/\partial V$  have a simple structure of a single peak while the resonances of  $\partial S^>/\partial V$  have a fine structure composed of two peaks. From numerical calculations we find that the distance between these two peaks is approximately equal to  $\Gamma$  and does not depend on the other parameters. In the lower panel we show the ratio  $(\partial S^>/\partial V)/(\partial I/\partial V)$  corresponding to the two curves in the upper panel. Note, while the variations of the  $\partial S^>/\partial V$  and  $\partial I/\partial V$  reach several orders of magnitude, their ratio changes relatively weakly and shows a number of characteristic features. Specifically, in the Majorana regime, that is for  $|eV| < |\eta_1|$ , this ratio is characterized by plateaus separated by an antiresonance located at  $|eV_{\text{res},2}|$ . At these plateaus the ratio is equal to  $3e/2$  and at the minimum of the antiresonance it is equal to  $e/2$ . Also at  $|eV_{\text{res},1}|$  there exists an antiresonance with the same minimum  $e/2$ . For very large bias voltages,  $|eV| \gg |\eta_1|$ , when the Majorana tunneling is ineffective, the two Majorana modes behave as a single Dirac fermion and there forms a trivial plateau with the Dirac value  $(\partial S^>/\partial V)/(\partial I/\partial V) = e$ .

#### IV. CONCLUSION

We have demonstrated how to reveal Majorana fractionalization using quantum transport characteristics such as differential shot noise and conductance in Majorana QD setups where both Majorana modes are entangled with a strongly nonequilibrium QD. Our numerical results show that the tunneling phases wash out the Majorana universal values of each of these two observables. At the same time it has been found that the ratio of the differential shot noise and conductance weakly depends on the tunneling phases and provides a reliable access to Majorana fractionalization in realistic strongly nonequilibrium setups. In particular, it has been explicitly demonstrated that this ratio takes fractional values when MBSs in a TS are well separated whereas the ratio becomes integer for strongly overlapping MBSs merging

into a single Dirac fermion. Additionally, we have demonstrated the universality of the Majorana fractionalization that is its independence not only of the tunneling phase difference  $\Delta\phi$  but also its independence of the QD gate voltage  $\epsilon_d$  and bias voltage  $V$ . Regarding the behavior of the differential shot noise and conductance we have found that each of these observables has a resonant structure in its dependence on both the tunneling phase difference and bias voltage. Fine structures of these resonances have been explicitly shown and explored.

Let us in conclusion probe the Majorana universality at high temperatures achievable in state-of-the-art experiments. The insets in the lower panel of Fig. 4 illustrate results obtained for  $k_B T/\Gamma = 10$ . At both of the insets  $\Delta\phi = \pi/512$  and the other parameters remain unchanged. The two curves in the right inset show  $\partial S^>/\partial V$  (solid) and  $\partial I/\partial V$  (dashed). The curve in the left inset shows the ratio  $(\partial S^>/\partial V)/(\partial I/\partial V)$  obtained from the two curves in the right inset. As one can see in the left inset, high temperatures destroy the low-energy part of the universal fractional Majorana plateau. However, for bias voltages in the range  $k_B T \ll |eV| < |\eta_1|$  the high-energy part of this plateau is still present and provides an experimental access to the universal fractional Majorana ratio  $3e/2$ .

Finally, we note that our results enable to extract all the Majorana tunneling parameters. Indeed, according to Eq. (13), one obtains  $|\eta_2|$  from measurements of  $\Delta\phi_{I,\text{max}}$  since the bias voltage  $V$  is known in experiments. Measuring then  $|eV_{\text{res},1}|$  and  $|eV_{\text{res},2}|$  one gets  $|\eta_1|$  and  $\Delta\phi$  using Eq. (15). Besides, the expression for  $|eV_{\text{res},2}|$  in Eq. (15) suggests that one may increase  $|\eta_2|$  as necessary to shift the corresponding Majorana resonances of  $\partial S^>/\partial V$  and  $\partial I/\partial V$  to higher bias voltages where it is easier to measure them at higher temperatures.

#### ACKNOWLEDGMENTS

The author thanks Reinhold Egger, Andreas K. Hüttel and Wataru Izumida for useful discussions.

- 
- [1] A. Yu. Kitaev, “Unpaired Majorana fermions in quantum wires,” *Phys.-Usp.* **44**, 131 (2001).
  - [2] E. Majorana, “Teoria simmetrica dell’elettrone e del positrone,” *Nuovo Cimento* **14**, 171 (1937).
  - [3] J. Alicea, “New directions in the pursuit of Majorana fermions in solid state systems,” *Rep. Prog. Phys.* **75**, 076501 (2012).
  - [4] M. Sato and S. Fujimoto, “Majorana fermions and topology in superconductors,” *J. Phys. Soc. Japan* **85**, 072001 (2016).
  - [5] R. M. Lutchyn, E. P. A. M. Bakkers, L. P. Kouwenhoven, P. Krogstrup, C. M. Marcus, and Y. Oreg, “Majorana zero modes in superconductor-semiconductor heterostructures,” *Nat. Rev. Mater.* **3**, 52 (2018).
  - [6] V. V. Val’kov, M. S. Shustin, S. V. Aksenov, A. O. Zlotnikov, A. D. Fedoseev, V. A. Mitskan, and M. Yu. Kagan, “Topological superconductivity and Majorana states in low-dimensional systems,” *Phys. Usp.* **65** (2022).
  - [7] A. Yu. Kitaev, “Fault-tolerant quantum computation by anyons,” *Ann. Phys.* **303**, 2 (2003).
  - [8] D. E. Liu and H. U. Baranger, “Detecting a Majorana-fermion zero mode using a quantum dot,” *Phys. Rev. B* **84**, 201308(R) (2011).
  - [9] E. Vernek, P. H. Penteado, A. C. Seridonio, and J. C. Egues, “Subtle leakage of a Majorana mode into a quantum dot,” *Phys. Rev. B* **89**, 165314 (2014).



- [10] J. P. Ramos-Andrade, O. Ávalos-Ovando, P. A. Orellana, and S. E. Ulloa, “Thermoelectric transport through Majorana bound states and violation of Wiedemann-Franz law,” *Phys. Rev. B* **94**, 155436 (2016).
- [11] C.-X. Liu, J. D. Sau, T. D. Stanescu, and S. Das Sarma, “Andreev bound states versus Majorana bound states in quantum dot-nanowire-superconductor hybrid structures: Trivial versus topological zero-bias conductance peaks,” *Phys. Rev. B* **96**, 075161 (2017).
- [12] S. Smirnov, “Dual Majorana universality in thermally induced nonequilibrium,” *Phys. Rev. B* **101**, 125417 (2020).
- [13] L. Hong, F. Chi, Z.-G. Fu, Y.-F. Hou, Z. Wang, K.-M. Li, J. Liu, H. Yao, and P. Zhang, “Large enhancement of thermoelectric effect by Majorana bound states coupled to a quantum dot,” *J. Appl. Phys.* **127**, 124302 (2020).
- [14] F. Chi, Z.-G. Fu, J. Liu, K.-M. Li, Z. Wang, and P. Zhang, “Thermoelectric effect in a correlated quantum dot side-coupled to Majorana bound states,” *Nanoscale Res. Lett.* **15**, 79 (2020).
- [15] L.-W. Tang and W.-G. Mao, “Detection of Majorana bound states by sign change of the tunnel magnetoresistance in a quantum dot coupled to ferromagnetic electrodes,” *Front. Phys.* **8**, 147 (2020).
- [16] G. Zhang and C. Spånslätt, “Distinguishing between topological and quasi Majorana zero modes with a dissipative resonant level,” *Phys. Rev. B* **102**, 045111 (2020).
- [17] F. Chi, T.-Y. He, J. Wang, Z.-G. Fu, L.-M. Liu, P. Liu, and P. Zhang, “Photon-assisted transport through a quantum dot side-coupled to Majorana bound states,” *Front. Phys.* **8**, 254 (2020).
- [18] T.-Y. He, H. Sun, and G. Zhou, “Photon-assisted Seebeck effect in a quantum dot coupled to Majorana zero modes,” *Front. Phys.* **9**, 687438 (2021).
- [19] F. Chi, T.-Y. He, and G. Zhou, “Photon-assisted average current through a quantum dot coupled to Majorana bound states,” *J. Nanoelectron. Optoelectron.* **16**, 1325 (2021).
- [20] Z.-H. Wang and W.-C. Huang, “Dual negative differential of heat generation in a strongly correlated quantum dot side-coupled to Majorana bound states,” *Front. Phys.* **9**, 727934 (2021).
- [21] P. Majek, K. P. Wójcik, and I. Weymann, “Spin-resolved thermal signatures of Majorana-Kondo interplay in double quantum dots,” *Phys. Rev. B* **105**, 075418 (2022).
- [22] N. Bondyopadhyaya and D. Roy, “Nonequilibrium electrical, thermal and spin transport in open quantum systems of topological superconductors, semiconductors and metals,” *J. Stat. Phys.* **187**, 11 (2022).
- [23] K. Wrześniewski and I. Weymann, “Magnetization dynamics in a Majorana-wire-quantum-dot setup,” *Phys. Rev. B* **103**, 125413 (2021).
- [24] D. E. Liu, M. Cheng, and R. M. Lutchyn, “Probing Majorana physics in quantum-dot shot-noise experiments,” *Phys. Rev. B* **91**, 081405(R) (2015).
- [25] D. E. Liu, A. Levchenko, and R. M. Lutchyn, “Majorana zero modes choose Euler numbers as revealed by full counting statistics,” *Phys. Rev. B* **92**, 205422 (2015).
- [26] A. Haim, E. Berg, F. von Oppen, and Y. Oreg, “Current correlations in a Majorana beam splitter,” *Phys. Rev. B* **92**, 245112 (2015).
- [27] S. Valentini, M. Governale, R. Fazio, and F. Taddei, “Finite-frequency noise in a topological superconducting wire,” *Physica E* **75**, 15 (2016).
- [28] S. Smirnov, “Non-equilibrium Majorana fluctuations,” *New J. Phys.* **19**, 063020 (2017).
- [29] S. Smirnov, “Universal Majorana thermoelectric noise,” *Phys. Rev. B* **97**, 165434 (2018).
- [30] S. Smirnov, “Majorana finite-frequency nonequilibrium quantum noise,” *Phys. Rev. B* **99**, 165427 (2019).
- [31] S. Smirnov, “Dynamic Majorana resonances and universal symmetry of nonequilibrium thermoelectric quantum noise,” *Phys. Rev. B* **100**, 245410 (2019).
- [32] G.-H. Feng and H.-H. Zhang, “Probing robust Majorana signatures by crossed Andreev reflection with a quantum dot,” *Phys. Rev. B* **105**, 035148 (2022).
- [33] A. Zazunov, R. Egger, and A. Levy Yeyati, “Low-energy theory of transport in Majorana wire junctions,” *Phys. Rev. B* **94**, 014502 (2016).
- [34] T. Jonckheere, J. Rech, A. Zazunov, R. Egger, A. Levy Yeyati, and T. Martin, “Giant shot noise from Majorana zero modes in topological trijunctions,” *Phys. Rev. Lett.* **122**, 097003 (2019).
- [35] J. Manousakis, C. Wille, A. Altland, R. Egger, K. Flensberg, and F. Hassler, “Weak measurement protocols for Majorana bound state identification,” *Phys. Rev. Lett.* **124**, 096801 (2020).
- [36] S. Smirnov, “Majorana tunneling entropy,” *Phys. Rev. B* **92**, 195312 (2015).
- [37] E. Sela, Y. Oreg, S. Plugge, N. Hartman, S. Lüscher, and J. Folk, “Detecting the universal fractional entropy of Majorana zero modes,” *Phys. Rev. Lett.* **123**, 147702 (2019).
- [38] S. Smirnov, “Majorana entropy revival via tunneling phases,” *Phys. Rev. B* **103**, 075440 (2021).
- [39] S. Smirnov, “Majorana ensembles with fractional entropy and conductance in nanoscopic systems,” *Phys. Rev. B* **104**, 205406 (2021).
- [40] M. Tanhayi Ahari, S. Zhang, J. Zou, and Y. Tserkovnyak, “Biasing topological charge injection in topological matter,” *Phys. Rev. B* **104**, L201401 (2021).
- [41] N. Hartman, C. Olsen, S. Lüscher, M. Samani, S. Fallahi, G. C. Gardner, M. Manfra, and J. Folk, “Direct entropy measurement in a mesoscopic quantum system,” *Nat. Phys.* **14**, 1083 (2018).
- [42] Y. Kleeorin, H. Thierschmann, H. Buhmann, A. Georges, L. W. Molenkamp, and Y. Meir, “How to measure the entropy of a mesoscopic system via thermoelectric transport,” *Nat. Commun.* **10**, 5801 (2019).
- [43] E. Pyurbeeva and J. A. Mol, “A thermodynamic approach to measuring entropy in a few-electron nanodevice,” *Entropy* **23**, 640 (2021).
- [44] T. Child, O. Sheekey, S. Lüscher, S. Fallahi, G. C. Gardner, M. Manfra, Y. Kleeorin, Y. Meir, and J. Folk, “Entropy measurement of a strongly correlated quantum dot,” arXiv:2110.14158 (2021).
- [45] T. Child, O. Sheekey, S. Lüscher, S. Fallahi, G. C. Gardner, M. Manfra, and J. Folk, “A robust protocol for entropy measurement in mesoscopic circuits,” *Entropy* **24**, 417 (2022).
- [46] C. Han, Z. Iftikhar, Y. Kleeorin, A. Anthore, F. Pierre, Y. Meir, A. K. Mitchell, and E. Sela, “Fractional entropy of multichannel Kondo systems from conductance-charge relations,” *Phys. Rev. Lett.* **128**, 146803 (2022).
- [47] V. Mourik, K. Zuo, S. M. Frolov, S. R. Plissard, E. P. A. M. Bakkers, and L. P. Kouwenhoven, “Signatures of Majorana fermions in hybrid superconductor-semiconductor nanowire devices,” *Science* **336**, 1003

- (2012).
- [48] P. Yu, J. Chen, M. Gomanko, G. Badawy, E. P. A. M. Bakkers, K. Zuo, V. Mourik, and S. M. Frolov, “Non-Majorana states yield nearly quantized conductance in proximatized nanowires,” *Nat. Phys.* **17**, 482 (2021).
- [49] S. Frolov, “Quantum computing’s reproducibility crisis: Majorana fermions,” *Nature* **592**, 350 (2021).
- [50] A. Kejriwal and B. Muralidharan, “Nonlocal conductance and the detection of Majorana zero modes: Insights from von Neumann entropy,” *Phys. Rev. B* **105**, L161403 (2022).
- [51] M. Gau, R. Egger, A. Zazunov, and Y. Gefen, “Towards dark space stabilization and manipulation in driven dissipative Majorana platforms,” *Phys. Rev. B* **102**, 134501 (2020).
- [52] M. Gau, R. Egger, A. Zazunov, and Yuval Gefen, “Driven dissipative Majorana dark spaces,” *Phys. Rev. Lett.* **125**, 147701 (2020).
- [53] M. T. Deng, S. Vaitiekėnas, E. B. Hansen, J. Danon, M. Leijnse, K. Flensberg, J. Nygård, P. Krogstrup, and C. M. Marcus, “Majorana bound state in a coupled quantum-dot hybrid-nanowire system,” *Science* **354**, 1557 (2016).
- [54] M.-T. Deng, S. Vaitiekėnas, E. Prada, P. San-Jose, J. Nygård, P. Krogstrup, R. Aguado, and C. M. Marcus, “Nonlocality of Majorana modes in hybrid nanowires,” *Phys. Rev. B* **98**, 085125 (2018).
- [55] D. C. Ralph and R. A. Buhrman, “Kondo-assisted and resonant tunneling via a single charge trap: A realization of the Anderson model out of equilibrium,” *Phys. Rev. Lett.* **72**, 3401 (1994).
- [56] D. Goldhaber-Gordon, H. Shtrikman, D. Mahalu, D. Abusch-Magder, U. Meirav, and M. A. Kastner, “Kondo effect in a single-electron transistor,” *Nature (London)* **391**, 156 (1998).
- [57] L. I. Glazman and M. E. Raikh, “Resonant Kondo transparency of a barrier with quasilocal impurity states,” *JETP Lett.* **47**, 452 (1988).
- [58] Y. Meir, N. S. Wingreen, and P. A. Lee, “Low-temperature transport through a quantum dot: The Anderson model out of equilibrium,” *Phys. Rev. Lett.* **70**, 2601 (1993).
- [59] N. S. Wingreen and Y. Meir, “Anderson model out of equilibrium: Noncrossing-approximation approach to transport through a quantum dot,” *Phys. Rev. B* **49**, 11040 (1994).
- [60] S. Smirnov and M. Grifoni, “Slave-boson Keldysh field theory for the Kondo effect in quantum dots,” *Phys. Rev. B* **84**, 125303 (2011).
- [61] S. Smirnov and M. Grifoni, “Kondo effect in interacting nanoscopic systems: Keldysh field integral theory,” *Phys. Rev. B* **84**, 235314 (2011).
- [62] R. López, M. Lee, L. Serra, and J. S. Lim, “Thermoelectrical detection of Majorana states,” *Phys. Rev. B* **89**, 205418 (2014).
- [63] D. A. Ruiz-Tijerina, E. Vernek, L. G. G. V. Dias da Silva, and J. C. Egues, “Interaction effects on a Majorana zero mode leaking into a quantum dot,” *Phys. Rev. B* **91**, 115435 (2015).
- [64] M. Leijnse and K. Flensberg, “Scheme to measure Majorana fermion lifetimes using a quantum dot,” *Phys. Rev. B* **84**, 140501(R) (2011).
- [65] M. Lee, J. S. Lim, and R. López, “Kondo effect in a quantum dot side-coupled to a topological superconductor,” *Phys. Rev. B* **87**, 241402(R) (2013).
- [66] M. Cheng, M. Becker, B. Bauer, and R. M. Lutchyn, “Interplay between Kondo and Majorana interactions in quantum dots,” *Phys. Rev. X* **4**, 031051 (2014).
- [67] I. Weymann and K. P. Wójcik, “Transport properties of a hybrid Majorana wire-quantum dot system with ferromagnetic contacts,” *Phys. Rev. B* **95**, 155427 (2017).
- [68] J. D. Cifuentes and L. G. G. V. Dias da Silva, “Manipulating Majorana zero modes in double quantum dots,” *Phys. Rev. B* **100**, 085429 (2019).
- [69] J. F. Silva, L. G. G. V. Dias da Silva, and E. Vernek, “Robustness of the Kondo effect in a quantum dot coupled to Majorana zero modes,” *Phys. Rev. B* **101**, 075428 (2020).
- [70] A. Altland and B. Simons, *Condensed Matter Field Theory*, 2nd ed. (Cambridge University Press, Cambridge, 2010).